RESEARCH ARTICLE

Functional Properties of $SrTi_{1-x}Fe_xO_3$ Dielectric Ceramics

M. Imran Khan[1,2,*], Fayaz Hussain[1,*], Hareem Zubairi[3], Syeda Mahnoor Fatima[1], Sajida Shaikh[1], Ikhtiar Hussain Bhellar[1,5], Fazli Akram[4], Ahmed Ali Bozdar[1,5], S. Naseem Shah[2], Mukhtiar Hussain[6] and Muhammad Fahad Riaz[7]

[1] Department of Materials Engineering, NED University of Engineering and Technology, Karachi 75270, Pakistan
[2] Department of Physics, Federal Urdu University of Arts, Science and Technology, Karachi 75300, Pakistan
[3] Department of Materials, The University of Manchester, M13 9PL, Manchester, United Kingdom
[4] Department of Materials and Metallurgical Engineering, New Mexico Institute of Mining and Technology, Socorro, NM 87801, United States
[5] Department of Physics, NED University of Engineering and Technology, Karachi 75270, Pakistan
[6] School of Materials Science and Engineering, Beijing Institute of Technology, Beijing 100081, China
[7] Department of Metallurgy and Materials Engineering, Dawood University of Engineering and Technology, Karachi 74800, Pakistan

Abstract

This study focuses on the solid-state processing optimization of $SrTi_{1-x}Fe_xO_3$ (STFO) ceramics with $0.00 \leq x \leq 0.11$. X-ray diffraction reveals a single-phase cubic structure (space group $Pm\bar{3}m$) with lattice constant $a = b = c = 3.91\,\text{Å}$ and a maximum relative density of ∼94%. SEM confirms well-formed grains in both pure and Fe^{3+}-doped $SrTiO_3$. TGA/DSC indicates low weight loss and high thermal stability for the $x = 0.09$ composition. Electrical conductivity increases with frequency, accompanied by higher dielectric losses for $x = 0.09$ and $x = 0.11$. FTIR verifies the Ti-O octahedral stretching frequency at $530\,\text{cm}^{-1}$, consistent with the cubic perovskite structure. The maximum Seebeck coefficient is observed at $x = 0.09$, aligning with electrical data and confirming semiconducting behavior. Notably, calcined powders exhibit soft ferromagnetic loops, whereas sintered solids display antiferromagnetic loops, revealing intriguing magnetic properties. Overall, the optimized $x = 0.09$ composition shows significant promise for applications requiring enhanced electrical and magnetic characteristics.

Keywords: eco-friendly, $SrTi_{1-x}Fe_xO_3$ perovskites, dielectric properties, Seebeck coefficient.

1 Introduction

Fe-doped STO is a p-type semiconductor material that can be used as a thermoelectric material at high temperature range. The significant rise in

Submitted: 20 January 2026
Accepted: 22 March 2026
Published: 26 March 2026

Vol. 2, **No.** 1, 2026.
10.62762/JAEM.2026.503292

***Corresponding authors:**
✉ M. Imran Khan
imrankhan25430@gmail.com
✉ Fayaz Hussain
fhussain@neduet.edu.pk

Citation
Khan, M. I, Hussain, F., Zubairi, H., Fatima, S. M., Shaikh, S., Bhellar, I. H., Akram, F., Bozdar, A. A., Shah, S. N., Hussain, M., & Riaz, M. F. (2026). Functional Properties of $SrTi_{1-x}Fe_xO_3$ Dielectric Ceramics. *Journal of Advanced Electronic Materials*, 2(1), 8–19.

research in thermoelectric ceramics has potential to tackle energy crises issues and miniaturization of power devices [1–5]. The devices based on these materials have niche applications and are used in space exploration devices. STO is an excellent perovskite having high melting point, a wider range of defect chemistry and exhibits semiconducting behavior on donor/acceptor doping [6–8]. Researchers have concentrated their efforts in the development of environmental friendly oxide ceramic having potential of utilization of wasted heat [9, 10]. The wasted energy (in the form of heat) released by electronics, factories, automobiles, and power plants is of great interest, and thermoelectric materials have received a lot of study for this purpose [11–16]. Particularly, the perovskite structure of strontium titanate ($SrTiO_3$), lead-free composition, results in an enhancement of desired properties, including excellent thermal and chemical stability, low dielectric loss, and a high dielectric constant [17]. Subsequently, it has gained widespread popularity as a versatile ceramic material extensively employed in diverse applications, including sensors, actuators, electro-optical devices, random-access memory, and multilayer capacitors [18, 19]. The synthesis method employed significantly influences the composition, structure, particle size distribution, crystal characteristics, and surface attributes of powders and ceramics [18]. Cubic $SrTiO_3$ (STO) of the perovskite-type may be doped to yield compounds with potential thermoelectric properties across a broad temperature range [20–24]. The popularity of $SrTiO_3$-based oxide thermoelectric materials has increased because of their low cost, non-toxicity, and high redox flexibility and thermal stability [25, 26]. When $SrTiO_3$ is doped with pentavalent elements at its B-site cation and trivalent elements at its A-site cation converts it from an insulator to a semiconductor [17, 22, 26–36]. A donor dopant with a stronger cationic charge, such as Ta^{5+} or Nb^{5+} [29, 36], is replaced for the host cation titanium (Ti^{4+}), which has a lower charge, to improve the electrical properties and overall performance of $SrTiO_3$ ceramics. This strategic substitution plays a crucial role in tailoring the electrical behavior of the ceramics for specific applications.

Polycrystalline ceramics yttrium (Y)-doped $Ca_3Co_4O_9$ ceramics have shown thermoelectric behavior even at low temperatures [37]. Heavily La and Nb-doped $SrTiO_3$ (STO) have shown a change in Thermoelectric performance (ZT of 0.27 at 1073K and La doping of 8.4×10^{20} cm^{-3}) with increasing carrier concentration [38]. Iron (Fe) or silver (Ag)-doped NaTaO3 ceramics have shown modified thermoelectric properties compared to pure $NaTaO_3$ [39]. Perovskite is an extraordinarily versatile structured material is an integral part of future developments in integrated technology [3, 15, 18, 30, 40–43]. This structure diversity of perovskites provides an extreme range of electrical, magnetic, optical, and mechanical properties over a wide temperature range [44]. Thermo-analytical measurements of perovskite, $CaTiO_3$, $BaTiO_3$, and $SrTiO_3$ have shown good thermal stability in the temperature range of 1000–1200°C [45]. Among these, the perovskites (ABO_3) structured materials exhibit an excellent ferroelectric response [46]. BiSbTe p-type, Ag-Sb, and K-doped PbTe p-type, SiGe, have been prepared by different methods having thermoelectric performance <1 but their optimum temperature of operation is low [47]. Fe-doped strontium titanate and the $Sr(Fe_{0.5}Ti_{0.5})$ perovskite have been prepared using the combustion synthesis method and sintered at 1250°C with no study of electrical and magnetic properties [17, 22–24, 27, 29, 31, 33–35, 48–56]. The transition metallic induction at A/B-site cations position in perovskite structure compound causes properties variation [21]. The devices based on these materials have various applications and are mostly used in space technologies [57–63]. STO is an excellent perovskite with a high melting point (2600°C), and a wider range of defect chemistry and exhibits semiconducting behavior on donor/acceptor doping [25, 68].

At room temperature, STO exists in the cubic perovskite structure with a lattice parameter of 0.3905 nm and a good insulator with a 3.2 eV band gap (at T= 10K) separating the valence band from the conduction band and density of 5.12 g/cm^3 [65]. This alteration changes the electrical conductivity in bulk STO single crystals [35]. The rapidly growing field of thermoelectric developed heavily doped semiconductor materials for commercial uses [66]. The electrical properties of perovskite structured ceramic oxide 'STO' can be tuned by the induction of heavy metal ions [35]. Recent research reveals that the electronic performance of STO may be enhanced by A or B site substitution [67] but none of it relates it to the magnetic properties and study the ferromagnetic behavior of the STO-based ceramics. Theoretical studies on Fe-doped $SrTiO_3$ have also revealed significant modifications in the electronic structure near the Fermi level, providing insight into the origin of its semiconducting behavior [64]. However, a

comprehensive experimental investigation linking microstructural evolution, electrical transport, and magnetic properties in $SrTi_{1-x}Fe_xO_3$ ceramics remains limited. The rationale of this work is to compare the microstructural, electrical, thermal, and magnetic properties by doping the STO compound with Fe, i.e., $SrTi_{1-x}Fe_xO_3$ (STFO) prepared by conventional solid-state sintering method. Substitution of Fe into STO reveals the promising thermoelectric (TE) material, promotes the structural changes in the STO, modify the magnetic properties, and enhances the electrical behavior as well. Solid-state energy conversion devices have smart features of long life, no moving parts and no toxic emission compared with conventional devices [68, 69].

2 Materials and Methods

The powder compositions of pure and doped $SrTi_{1-x}Fe_xO_3$, where $0.00 \leq x \leq 0.11$, were prepared by the conventional solid-state synthesis method. The precursors with high purity Strontium carbonate ($SrCO_3$) (Chemosavers, 99.8%, fine powder), Titanium oxide (TiO_2) (LOUDWOLF, 99.9%, 44-micron size), and Iron oxide (Fe_2O_3) (Eisen Golden Laboratories, 99.7%, fine powder size) were dried for 3 hrs at $300\,^{\circ}C$ following the by-weight batch calculation and mixing of 50 gm batches for each composition. Yttrium Stabilized Zirconia balls of different diameters were used as grinding media [70]. The powder compositions were mixed in ethanol and subjected to ball milling for 1 hr both before and after calcination to ensure homogeneous mixing. Subsequently, the mixture was dried at $80\,^{\circ}C$ to remove ethanol. The alcohol-free mixture was calcined at $900\,^{\circ}C$ using an alumina crucible by placing the crucible in a "Protherm Box Furnace" for 4 hrs to remove volatile impurities and formation of phases among the precursors. Approximately 2% of Polyvinyl Alcohol (PVA) solution was utilized as the organic binder, relative to the weight of the ceramic powder. Green pellets with a diameter of 12.7 mm and a weight of one gram were prepared by pressing the calcined powder at 200 MPa for 2 minutes. The green pellets were subjected to high temperature ($600\,^{\circ}C$ for 80 minutes) to evaporate the binder in the furnace followed by sintering at $1390\,^{\circ}C$ for 2hrs holding times (with $5\,^{\circ}C\,min^{-1}$ heating rate and $5\,^{\circ}C\,min^{-1}$ cooling rate). The structural characterization was done using the X-Ray Diffraction (XRD) peaks analysis on an X-Pert PRO diffractometer system equipped with Cu-Kα radiation ($\lambda = 1.5406\,Å$) in the 2θ range from $10°$ to $80°$ working at 40 kV and 30 mA with the step size of $0.02°$ or similar and continuous scan time was carried out on sintered pellets. The microstructural characterization was evaluated using the Scanning Electron Microscope (SEM) analysis (by using the JEOL JSM 6380L model) on the plane and fractured surfaces were performed. Fourier Transform Infrared (FTIR) analysis, model no. NICOLET IS50 was carried out using sintered powder compositions to evaluate the bonding between the metal-oxygen by the IR spectra concerning the wave number with the transmittance (%). To study the thermal properties, transition, and weight loss behavior of the compounds, TGA/DSC analysis (by using the model SDT/Q600, USA) was performed on pure STO and STFO powder compositions. Sample preparation for electrical measurements was done by applying silver electrodes on both sides of sintered polished pellets. The dielectric properties were studied using the Inductance, Capacitance, and Resistance (LCR) meter (by using the Tonghui, TH2826 model) to calculate the permittivity and conductance of the samples. Conductance and capacitance values of sintered pellets were obtained at a wider frequency range (25 kHz to 1 MHz). Electrical conductivity and relative permittivity were calculated using corresponding formulations. The thermoelectric (TE) properties were studied using the Seebeck coefficient measurements of p-type compositions and were performed using a Keithley voltmeter. Sintered samples were placed in locally developed ceramic devices open at both ends for smooth heat flow and having cylindrical diameter with a size comparable to the size of sintered pellets. A stack of four pellets was placed inside the device. K-type thermocouples were used to measure by creating a temperature gradient (hot and cold), respectively. High-temperature readings were obtained from the Keithley voltmeter and low-temperature readings were obtained using a Digital voltmeter. Voltage readings were obtained from the Keithley voltmeter in mV. Vibrating-Sample-Magnetometer (VSM) was used (by using the Microsense EZ-9) to generate magnetic hysteresis loops at -23 to $+23$ kOe applied magnetic field.

3 Results and Discussion

Figure 1 shows the structural analysis of STFO ceramic, where $0.00 \leq x \leq 0.11$, sintered compositions via XRD profiles. The characteristic peaks corresponding to planes shown in the figure indicate the formation of a cubic perovskite. The weak interaction between induced Fe^{3+} ions and O^{2-} ions as compared to Ti^{4+} and O^{2-} ions is evident from characteristic peaks as

Table 1. The density and lattice parameters of $SrTi_{1-x}Fe_xO_3$ calcined powder compositions using Rietveld Refinement by Highscore Plus (PDF4+ - 2022).

Composition (Value of x)	ICDD No. (used for Rietveld Analysis)	Crystal Structure/ Space Group	Lattice Parameters (Å)	The Volume of the Cell (Å^3)	Theoretical Density (g/cm^3)	Bulk Density (g/cm^3)	Relative Density (%)
0.00	04-012-6379		3.91	59.776	5.0981	4.3546	85.41
0.01	04-010-2592		3.9090	59.731	5.1097	4.4055	86.208
0.03	04-010-2592		3.905	59.547	5.1232	4.5500	88.811
0.05	04-010-2592	Cubic / Pm-3m	3.901	59.365	5.1391	4.7241	91.92
0.07	04-010-2592		3.8950	59.091	5.1736	4.8647	94.029
0.09	04-010-2592		3.87	57.961	5.2831	4.9463	93.624
0.11	04-010-2592		3.85	57.067	5.3648	4.9737	92.709

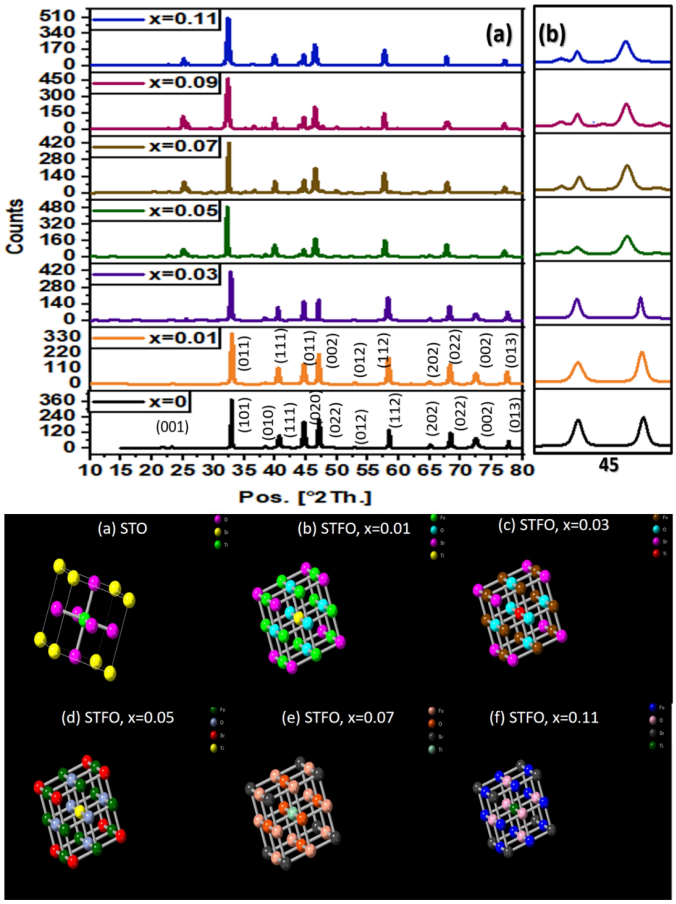

Figure 1. (a) X-ray diffraction patterns for sintered $SrTi_{1-x}Fe_xO_3$ ceramics (b) 45º peak (c) Crystallographic phase structure of pure SrTiFeO3 and Fe doped composition (a)-(f).

the ionic radii of Fe^{3+} (0.645 Å) are larger than that of Ti^{4+} (0.605 Å). The obtained structures exhibit the peak characteristics of the perovskite phase of strontium iron titanate. The crystallographic data were obtained, summarized in Table 1, as cubic symmetry space group $Pm\bar{3}m$ [24]. The lattice parameters and unit-cell volume for STO were obtained from Rietveld refinement using Highscore Plus, and these values were used in CrystalMaker (CM) software to calculate the theoretical density. The slight change in lattice constant with Fe^{3+} content confirms the successful substitution of Ti^{4+} by Fe^{3+} ions without changing the crystal structure. Also, Table 1 represents the theoretical and bulk densities of the STO ceramics and shows the maximum relative density on increasing doping level, indicating the increment of Fe^{3+} content in STO compound is increasing the relative densities [12, 36, 71–74]. The increase in relative density indicates better densification during sintering. This suggests that Fe substitution improves diffusion and packing of grains, resulting in more compact and stable ceramic structure.

The crystal structures shown in Figure 1(a–f) were modeled using CrystalMaker software based on the refined lattice parameters, illustrating the gradual substitution of Fe^{3+} ions at Ti^{4+} sites without distortion of the cubic perovskite framework. The simulated structures clearly confirm that increasing Fe concentration ($0.00 \leq x \leq 0.09$) preserves the $Pm\bar{3}m$ cubic symmetry while slightly modifying the lattice dimensions, supporting the XRD results.

The microstructural morphology of Fe^{3+} doped STO ceramics was observed using SEM at 5000X magnification. SEM images for all STFO compositions are shown in Figure 2(a–f). All compositions show smooth surface morphology and densified structure with increasing Fe^{3+} content in the STO-based ceramics. Fe^{3+} doped $SrTiO_3$ compositions exhibit prominent grain structures [75]. The lighter-colored region in 9% and 11% compositions reveals the presence of perovskite matrix grains. Fe^{3+} doped compositions show increased grain size by Fe^{3+} induction as the particles diffused into each other from the 10 μm to 16 μm range.

Thermal analysis TGA/DSC for pure $SrTiO_3$ and Fe^{3+} doped $SrTiO_3$ powder compositions was performed using the Universal V4.4A program. Thermal gravimetric analysis (TGA) depicting weight loss for all compositions from room temperature up to

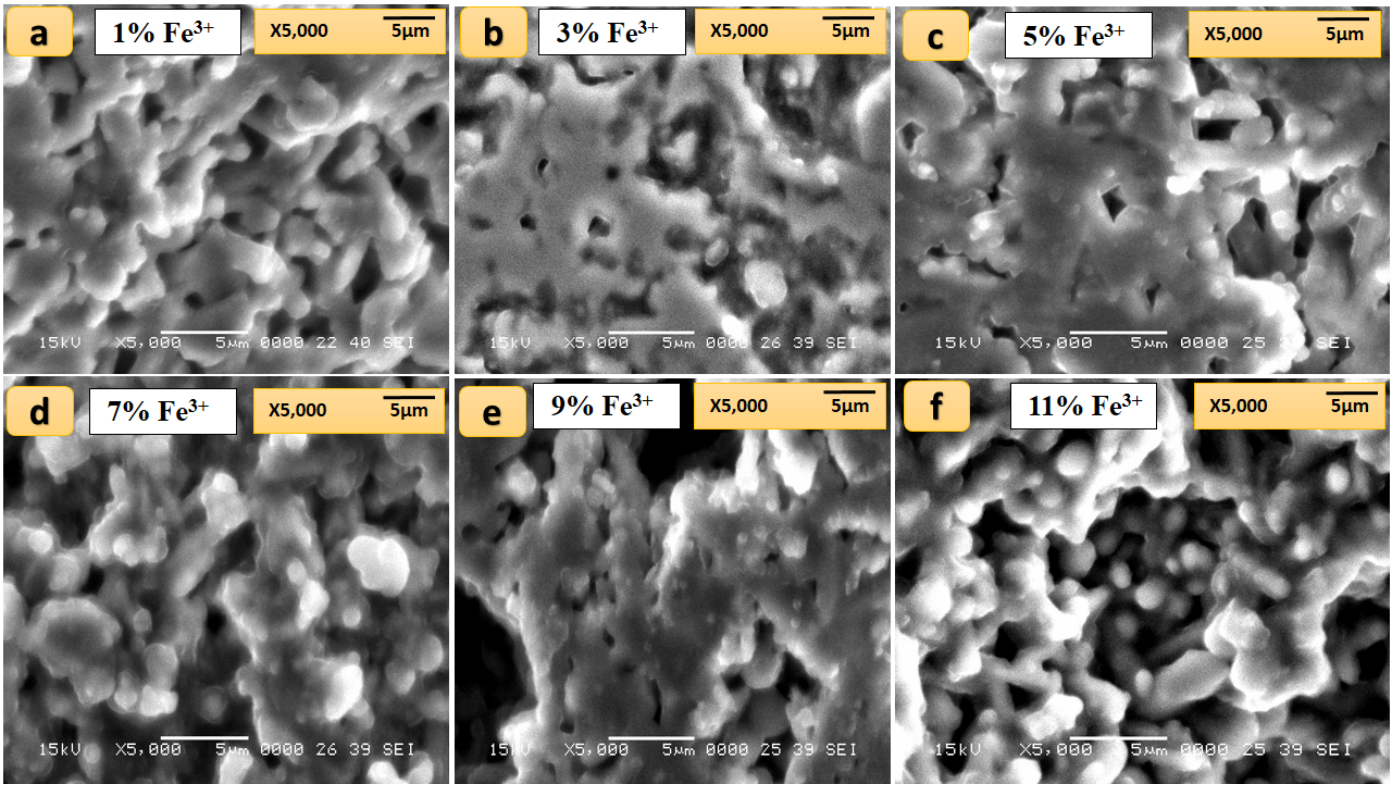

Figure 2. SEM micrographs of $SrTi_{1-x}Fe_xO_3$ ceramics for (a) $x = 0.00$, (b) $x = 0.01$, (c) $x = 0.03$, (d) $x = 0.05$, (e) $x = 0.07$, and (f) $x = 0.09$.

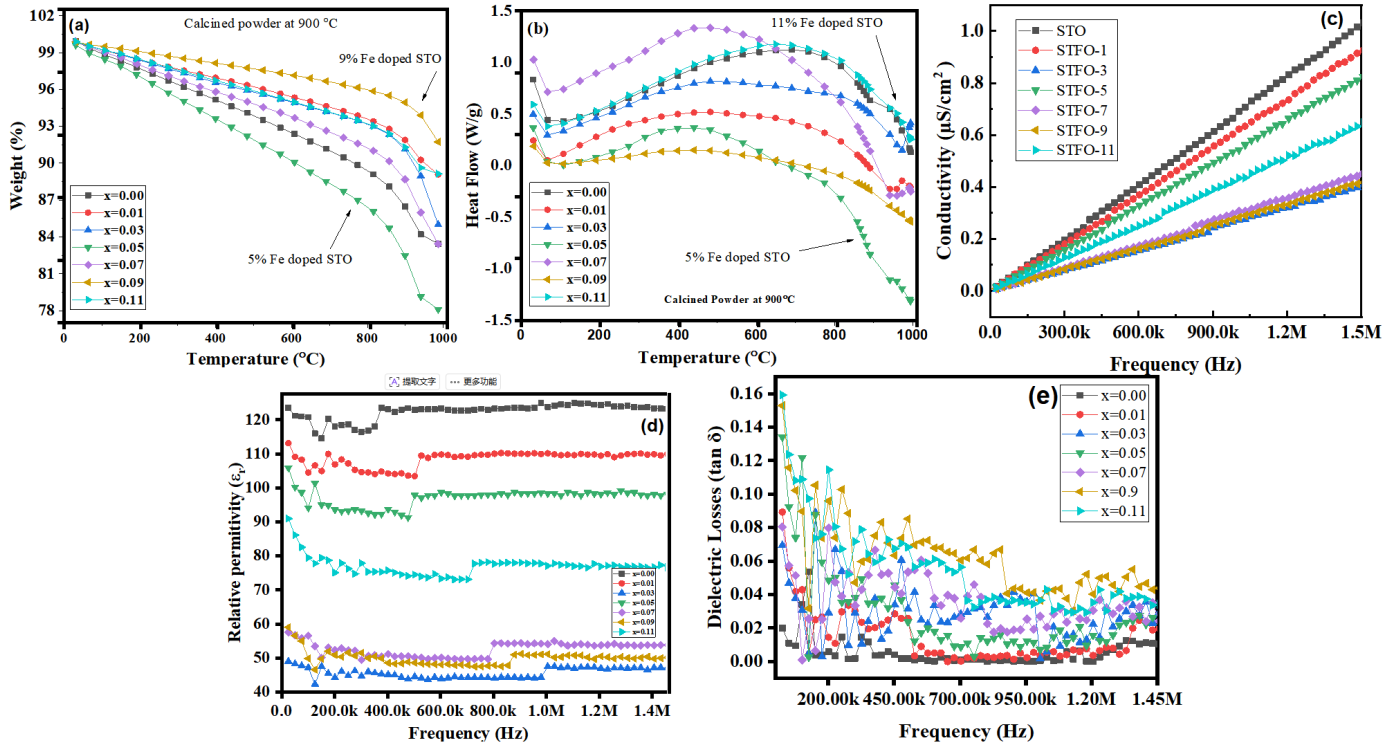

Figure 3. Results of $SrTi_{1-x}Fe_xO_3$ ceramics (a) TGA of calcined powder (b) DSC of calcined powder (c) Electrical conductivity vs frequency of sintered pellets (d) Relative permittivity vs Frequency of sintered pellets (e) Dielectric Losses vs Frequency of sintered pellets.

1000 °C is shown in Figure 3(a). A weight loss of 10–25% was observed in prepared compositions up to 1000 °C. 9% STFO ceramic exhibited the least and 5% STFO composition the most thermal

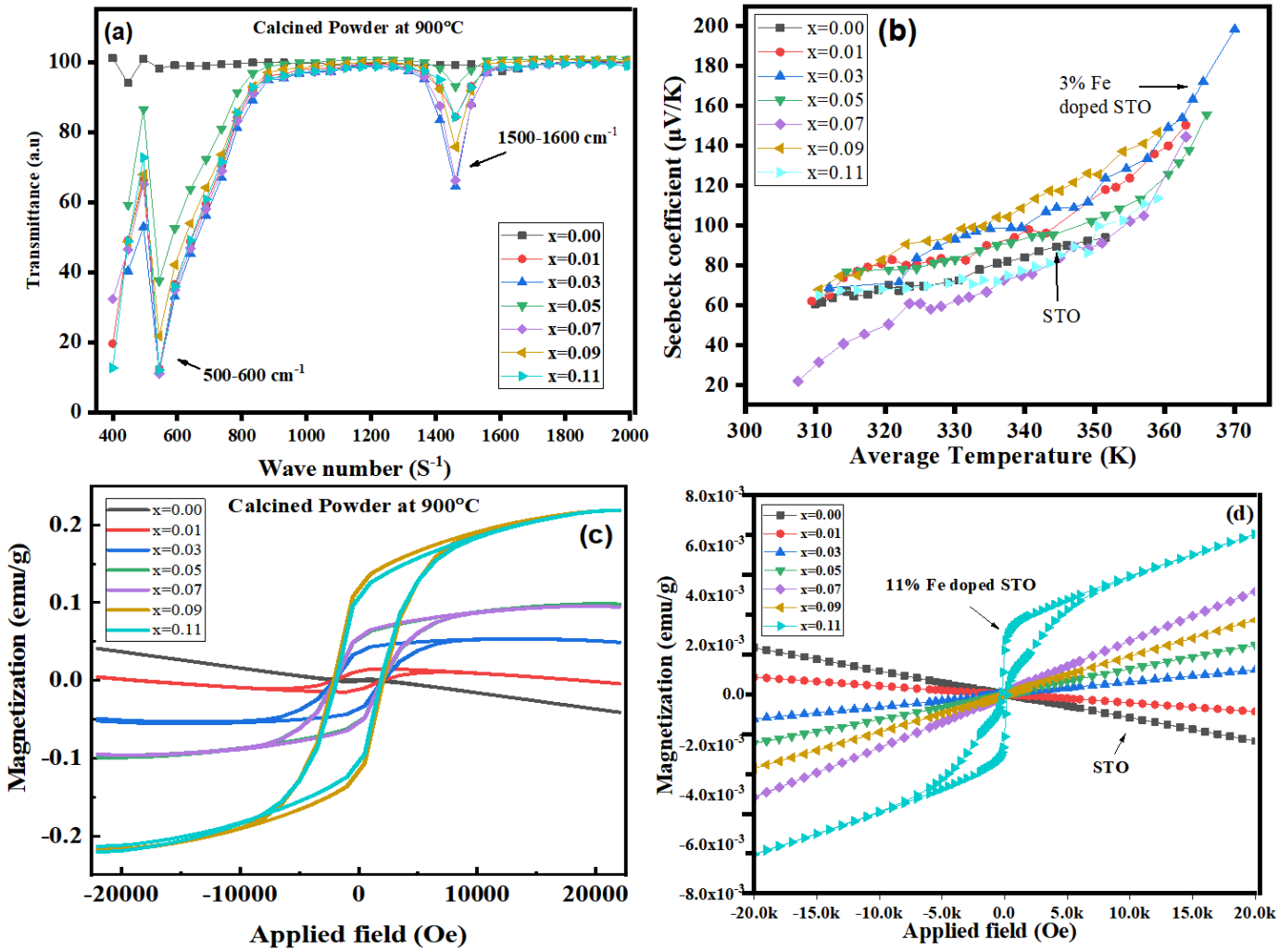

Figure 4. Results of $SrTi_{1-x}Fe_xO_3$ ceramics (a) FTIR (calcined powder) (b) Seebeck coefficient (c) Magnetization vs applied magnetic field (calcined powder) (d) Magnetization vs applied magnetic field.

decomposition showing the weak endothermic peak at around 830 °C. The heat flow in powder compositions is shown in the Differential Scanning calorimetry (DSC) curve in Figure 3(b). The presence of peaks at 100 °C to 120 °C reveals dehydration weight loss [74, 76] and phase transition [20]. The peaks between 800 °C to 1000 °C attributed to organic compound decomposition indicating that this composition isn't reacting up to 830 °C [77–81].

Electrical conductance versus frequency response for sintered pellet $SrTi_{1-x}Fe_xO_3$ compositions obtained from 400 Hz to 3 MHz using LCR meter. Formulated electrical conductivity (σ) vs frequency for all compositions is shown in Figure 3(c). Controlled composition $SrTiO_3$ ($x = 0.00$) and 11% Fe^{3+} ($x = 0.11$) doped $SrTiO_3$ results in the ~1.0 μS.cm^{-1} and ~0.6 μS.cm^{-1} at 1.5 MHz respectively. Electrical conductivity at lower frequencies exhibited less increase whereas higher values of conductivity were observed in higher values frequencies (in MHz) [35].

The capacitance versus frequency response for sintered and coated with silver electrode pellet $SrTi_{1-x}Fe_xO_3$ compositions obtained from 1 kHz to 100 kHz. Formulated relative permittivity (ε_r) vs frequency for all compositions is shown in Figure 3(d). The dielectric property of compositions remains linear up to 1.5 MHz [82]. The relative permittivity of Fe^{3+} doped $SrTiO_3$ decreased from ~120 (for $x = 0.00$) to ~50 (for $x = 0.09$) with a maximum of ~16% of dielectric losses in $SrTiO_3$ doped with 9% of Fe^{3+}. The increasing doping (Fe^{3+}) concentration in the base compound (STO) decreases the dielectric behavior [83]. There is a linear relationship between the frequency and the dielectric constant and dielectric loss tangent. The dielectric constant and the dielectric loss tangent decrease as the Fe doping level increases [26, 34, 73]. High dielectric characteristics are seen at low frequencies. The resistance drops with increasing

temperature, proving that the produced samples are semiconductors. Due to the rise in Fe carrier concentration, the conductivity of the entire series decreased.

Furthermore, FTIR spectroscopy for $SrTi_{1-x}Fe_xO_3$ calcined powder compositions was done for analysis of crystal lattices vibration at a wide frequency range. The variation in absorption peaks from $500\,cm^{-1}$ to $600\,cm^{-1}$ reveals Ti-O vibrations in STFO ceramics shown in Figure 4(a). Each peak has its own unique set of constraints (amplitude, FWHM, and spectral peak locations) that correspond to the precise type of vibration it represents within a certain structural group/spectral area. In all STFO samples, Ti-O bond vibrations occur within $500\,cm^{-1}$ to $550\,cm^{-1}$ in the STO perovskite structure material [84]. This minor change can be attributed by the random grain sizes and boundaries alignments [78, 85–88] relating it to phonon wave vector which in results providing the crystallographic axis arbitrarily dissemination.

Moreover, the potential gradient of sintered $SrTi_{1-x}Fe_xO_3$ compositions was measured using a Keithley voltmeter up to 370 K temperature. Positive voltages were observed for all compositions confirming p-type behavior [89]. The graph of thermoelectric volt measured from 280 K to 370 K temperature for pure and Fe^{3+} doped $SrTiO_3$ is shown in Figure 4(b). In the study, pure $SrTiO_3$ compositions exhibited the lowest voltage of 90 μV/K at a temperature of 358 K. On the other hand, the composition with 9% Fe^{3+} doping demonstrated the highest voltage of 270 μV/K at a temperature of 370 K. The graphical analysis reveals an intrinsic conducting behavior in Fe^{3+} doped compositions as the temperature increases.

4 Conclusion

In this study, we investigated $SrTi_{1-x}Fe_xO_3$ ceramics with varying Fe^{3+} content ($0.00 \leq x \leq 0.11$) prepared through conventional sintering at an optimized temperature of approximately 1390 °C. The XRD analysis confirmed the successful synthesis of single-phase cubic structures for all the $SrTi_{1-x}Fe_xO_3$ compositions, while SEM analysis revealed distinct morphological variations due to Fe^{3+} doping. Thermal analysis using TGA and DSC demonstrated the exceptional thermal stability of the prepared samples across a wide range from room temperature to 1000 °C. Furthermore, FTIR analysis confirmed the presence of perovskite structures in the $SrTi_{1-x}Fe_xO_3$ ceramics, evident from absorption peaks at wave number $530\,cm^{-1}$. In addition, Seebeck measurements revealed an enhancement in thermoelectric potential with rising temperatures. Moreover, the magnetic properties exhibited significant variations due to Fe^{3+} doping in $SrTiO_3$, with the maximum magnetic values observed when Fe^{3+} was doped at $x = 0.11$ in $SrTi_{1-x}Fe_xO_3$ ceramics.

Overall, the present findings suggest that $SrTi_{1-x}Fe_xO_3$ ceramic system holds tremendous potential for the development of high-performance, lead-free ceramics. These materials effectively address the co-existence of electrical and magnetic properties while enhancing densification without compromising existing properties. This study contributes valuable insights to the materials science and engineering field, paving the way for advanced applications and functional devices based on these engineered ceramics.

Data Availability Statement

Data will be made available on request.

Funding

This work was supported by the Internal Funding Program of the Materials Engineering Department, NED University of Engineering & Technology, Karachi, Pakistan.

Conflicts of Interest

The authors declare no conflicts of interest.

AI Use Statement

The authors declare that no generative AI was used in the preparation of this manuscript.

Ethical Approval and Consent to Participate

Not applicable.

References

[1] Ohtaki, M. (2011). Recent aspects of oxide thermoelectric materials for power generation from mid-to-high temperature heat source. *Journal of the Ceramic Society of Japan, 119*(1395), 770-775. [CrossRef]

[2] Koumoto, K., Wang, Y., Zhang, R., Kosuga, A., & Funahashi, R. (2010). Oxide thermoelectric materials: a nanostructuring approach. *Annual review of materials research, 40*(1), 363-394. [CrossRef]

[3] Srivastava, D., Norman, C., Azough, F., Schäfer, M. C., Guilmeau, E., & Freer, R. (2018). Improving the thermoelectric properties of SrTiO3-based ceramics with metallic inclusions. *Journal of Alloys and Compounds, 731*, 723-730. [CrossRef]

[4] Xiang, X., Zhu, Y., Zheng, J., Li, Y., Zhang, T., Gao, J., & Zhang, H. (2025). Interfacial Field Screening Governs Tribocatalysis in Nb-Doped SrTiO3. *Surfaces and Interfaces*, 108053. [CrossRef]

[5] Kahaly, M. U., & Schwingenschlögl, U. (2014). Thermoelectric performance enhancement of SrTiO 3 by Pr doping. *Journal of Materials Chemistry A, 2*(27), 10379-10383. [CrossRef]

[6] Wang, H. X., Wang, X. L., Bu, T. A., Xu, S. S., Lv, P. P., Ren, L. C., ... & Zhao, W. Y. (2025). A-site defect construction in medium-entropy SrTiO3 ceramics for enhanced thermoelectric performance. *Rare Metals, 44*(5), 3324-3338. [CrossRef]

[7] Egilmez, M., Leung, G. W., Hakimi, A. M. H. R., & Blamire, M. G. (2010). Origin of magnetism in La and Fe doped SrTiO3-δ films. *Journal of Applied Physics, 108*(12). [CrossRef]

[8] Prasanth, S. C., Vijay, A., Jose, R., & Saravanan, K. V. (2023). Liquid phase sintering of Nb doped SrTiO3-δ ceramics with enhanced thermoelectric figure of merit. *Ceram. Int.*, 104908. [CrossRef]

[9] Koumoto, K., Funahashi, R., Guilmeau, E., Miyazaki, Y., Weidenkaff, A., Wang, Y., & Wan, C. (2013). Thermoelectric ceramics for energy harvesting. *Journal of the American Ceramic Society, 96*(1), 1-23. [CrossRef]

[10] Wang, Q., Zhou, Z., Liu, C., Zheng, Y., Shi, Z., Wei, B., ... & Lin, Y. H. (2026). Advances in oxide thermoelectric materials: strategies, applications and beyond. *Chemical Society Reviews*.[CrossRef]

[11] Hui, S. (2000). *Evaluation of yttrium-doped $SrTiO_3$ as a solid oxide fuel cell anode* (Doctoral dissertation, McMaster University). McMaster University MacSphere Repository. Available at: http://hdl.handle.net/11375/6342

[12] Rothschild, A., Menesklou, W., Tuller, H. L., & Ivers-Tiffee, E. (2006). Electronic structure, defect chemistry, and transport properties of SrTi1-x Fe x O3-y solid solutions. *Chemistry of materials, 18*(16), 3651-3659. [CrossRef]

[13] Zhang, Y., & Stucky, G. D. (2014). Heterostructured approaches to efficient thermoelectric materials. *Chemistry of Materials, 26*(1), 837-848. [CrossRef]

[14] Hasan, T., Saha, A., Khan, M. N. I., Rashid, R., Basith, M. A., Bashar, M. S., & Ahmed, I. (2022). Structural, electrical, and magnetic properties of Ce and Fe doped SrTiO3. *AIP Advances, 12*(9).[CrossRef]

[15] He, J., Lu, X., Zhu, W., Hou, Y., Ti, R., Huang, F., ... & Zhu, J. (2015). Induction and control of room-temperature ferromagnetism in dilute Fe-doped SrTiO3 ceramics. *Applied Physics Letters, 107*(1). [CrossRef]

[16] Talanov, M. V., Stash, A. I., Ivanov, S. A., Zhukova, E. S., Gorshunov, B. P., Nekrasov, B. M., ... & Bush, A. A. (2024). Transition metal-doped SrTiO 3: when does a tiny chemical impact have such a great structural response?. *Journal of Materials Chemistry C, 12*(22), 8105-8118. [CrossRef]

[17] Bian, W., Lu, X., Li, Y., Min, C., Zhu, H., Fu, Z., & Zhang, Q. (2018). Influence of Nd doping on microwave dielectric properties of SrTiO3 ceramics. *Journal of Materials Science: Materials in Electronics, 29*(4), 2743-2747. [CrossRef]

[18] Živojinović, J., Peleš-Tadić, A., Kosanović, D., Dinić, I., Vuković, M., & Obradović, N. (2024). Photocatalytic degradation of tetracycline by Fe-doped mechanically activated SrTiO3 powders in aqueous solution. *Science of Sintering, 56*(4), 535-549. [CrossRef]

[19] Mohammed, A. A., & Ghaleb, A. M. (2025). Based on DFT Calculations, Some Physical Properties of The Perovskite Compound (SrTiO3) were Calculated. *Central Asian Journal of Theoretical and Applied Science, 6*(4), 791-807. [CrossRef]

[20] Baker, J. N., Bowes, P. C., Long, D. M., Moballegh, A., Harris, J. S., Dickey, E. C., & Irving, D. L. (2017). Defect mechanisms of coloration in Fe-doped SrTiO3 from first principles. *Applied Physics Letters, 110*(12). [CrossRef]

[21] Singh, S. P., Kanas, N., Desissa, T. D., Johnsson, M., Einarsrud, M. A., Norby, T., & Wiik, K. (2020). Thermoelectric properties of A-site deficient La-doped SrTiO3 at 100–900° C under reducing conditions. *Journal of the European Ceramic Society, 40*(2), 401-407. [CrossRef]

[22] Wang, Y. F., Lee, K. H., Ohta, H., & Koumoto, K. (2008). Fabrication and thermoelectric properties of heavily rare-earth metal-doped SrO (SrTiO3) n (n= 1, 2) ceramics. *Ceramics international, 34*(4), 849-852. [CrossRef]

[23] Ghosh, A., Masud, M. G., Sannigrahi, J., & Chaudhuri, B. K. (2013). Resistive transition, polaron dynamics and scaling behavior in Fe doped SrTiO3. *Physica B: Condensed Matter, 414*, 60-66. [CrossRef]

[24] Srivastava, D., Norman, C., Azough, F., Schäfer, M. C., Guilmeau, E., Kepaptsoglou, D., ... & Freer, R. (2016). Tuning the thermoelectric properties of A-site deficient SrTiO 3 ceramics by vacancies and carrier concentration. *Physical Chemistry Chemical Physics, 18*(38), 26475-26486. [CrossRef]

[25] Ohta, H. (2007). Thermoelectrics based on strontium titanate. *Materials today, 10*(10), 44-49. [CrossRef]

[26] Devi, N. Y., Vijayakumar, K., Rajasekaran, P., Nedunchezhian, A. A., Sidharth, D., Masaru, S., ... & Jayavel, R. (2021). Effect of Gd and Nb co-substitution on enhancing the thermoelectric power factor of nanostructured SrTiO3. *Ceramics International, 47*(3), 3201-3208. [CrossRef]

[27] Wang, Q., Zhang, W., Peng, B., & Zhang, W. (2017).

Inverse spin Hall effects in Nd doped SrTiO3. *AIP Advances, 7*(12). [CrossRef]

[28] Shan, K., Zhai, F., Li, N., & Yi, Z. Z. (2019, November). Electrical properties of La and Sm Co-doped SrTiO3 for mixed ionic-electronic conductor. In *IOP Conference Series: Materials Science and Engineering* (Vol. 678, No. 1, p. 012139). IOP Publishing. [CrossRef]

[29] Muta, H., Kurosaki, K., & Yamanaka, S. (2003). Thermoelectric properties of rare earth doped SrTiO3. *Journal of Alloys and Compounds, 350*(1-2), 292-295. [CrossRef]

[30] Živojinović, J., Tadić, A. P., Kosanović, D., Petrović, J., Filipović, S., Blagojević, V., & Obradović, N. (2025). The influence of Fe-doping on the structural, electrical and magnetic behavior of mechanically activated SrTiO3 ceramics. *Journal of Alloys and Compounds, 1010*, 177545. [CrossRef]

[31] Singh, S., Singh, P., Viviani, M., & Presto, S. (2018). Dy doped SrTiO3: A promising anodic material in solid oxide fuel cells. *international journal of hydrogen energy, 43*(41), 19242-19249. [CrossRef]

[32] Wang, X., Hu, Q., Li, L., & Lu, X. (2012). Effect of Pr substitution on structural and dielectric properties of SrTiO3. *Journal of Applied Physics, 112*(4). [CrossRef]

[33] Li, Y., Niu, S., Hao, Y., Zhou, W., Wang, J., & Liu, J. (2022). Role of oxygen vacancy on activity of Fe-doped SrTiO3 perovskite bifunctional catalysts for biodiesel production. *Renewable Energy, 199*, 1258-1271. [CrossRef]

[34] Tkach, A., Okhay, O., Almeida, A., & Vilarinho, P. M. (2017). Giant dielectric permittivity and high tunability in Y-doped SrTiO3 ceramics tailored by sintering atmosphere. *Acta Materialia, 130*, 249–260. [CrossRef]

[35] Tomio, T., Miki, H., Tabata, H., Kawai, T., & Kawai, S. (1994). Control of electrical conductivity in laser deposited SrTiO3 thin films with Nb doping. *Journal of Applied Physics, 76*(10), 5886-5890. [CrossRef]

[36] Li, R., Zhang, C., Liu, J., Zhou, J., & Xu, L. (2019). A review on the electrical properties of doped SrTiO3 as anode materials for solid oxide fuel cells. *Materials Research Express, 6*(10), 102006. [CrossRef]

[37] Mroziński, A., Molin, S., Karczewski, J., Kamecki, B. J., & Jasinski, P. (2019). The influence of iron doping on performance of $SrTi_{1-x}Fe_xO_3$-δ perovskite oxygen electrode for SOFC. *Electrochemical Society Transactions, 91*(1), 1299-1307. [CrossRef]

[38] Ohta, S., Nomura, T., Ohta, H., & Koumoto, K. (2005). High-temperature carrier transport and thermoelectric properties of heavily La-or Nb-doped SrTiO3 single crystals. *Journal of applied physics, 97*(3). [CrossRef]

[39] Sfirloaga, P., Marin, C. N., Malaescu, I., & Vlazan, P. (2016). The electrical performance of ceramics materials with perovskite structure doped with metallic ions. *Ceramics International, 42*(16), 18960-18964. [CrossRef]

[40] Zhu, Y., Peng, Y., & Du, X. (2024). Optimization of thermoelectric properties for microwave sintered Fe-doped ZnO. *Ceramics International, 50*(21), 43452-43457. [CrossRef]

[41] Opazo, M. A., Ong, S. P., Vargas, P., Ross, C. A., & Florez, J. M. (2019). Oxygen-vacancy tuning of magnetism in SrTi 0.75 Fe 0.125 Co 0.125 O 3-δ perovskite. *Physical Review Materials, 3*(1), 014404. [CrossRef]

[42] Shafique, H., Aldaghfag, S. A., Kashif, M., Zahid, M., Yaseen, M., Iqbal, J., & Neffati, R. (2021). Magnetic and optical characteristics of Fe doped SrTiO3 perovskite compound: a first principle study. *Chalcogenide Letters, 18*(10), 589-599. [CrossRef]

[43] Bhoyar, D. N., Kounsalye, J. S., Khirade, P. P., Pandit, A. A., & Jadhav, K. M. (2019). Doping effect of Fe ions on the structural, electrical, and magnetic properties of SrTiO3 nanoceramic matrix. *Journal of Superconductivity and Novel Magnetism, 32*(5), 1395-1406. [CrossRef]

[44] Bhalla, A. S., Guo, R., & Roy, R. (2000). The perovskite structure—a review of its role in ceramic science and technology. *Materials research innovations, 4*(1), 3-26. [CrossRef]

[45] Rothschild, A., Litzelman, S. J., Tuller, H. L., Menesklou, W., Schneider, T., & Ivers-Tiffée, E. (2005). Temperature-independent resistive oxygen sensors based on SrTi1-xFexO3-δ solid solutions. *Sensors and Actuators B: Chemical, 108*(1-2), 223-230. [CrossRef]

[46] Jung, K. H., Choi, S. M., & Seo, W. S. (2011). High temperature thermoelectric properties of Sr and Fe doped SmCoO3 perovskite structure. *Current Applied Physics, 11*(3), S260-S265. [CrossRef]

[47] Kovalevsky, A. V. (2017). Defects engineering for performing SrTiO3-based thermoelectric thin films: principles and selected approaches. In *Advanced Ceramic and Metallic Coating and Thin Film Materials for Energy and Environmental Applications* (pp. 91-120). Cham: Springer International Publishing. [CrossRef]

[48] Da Silva, L., Bernardi, M., Maia, L., Frigo, G., & Mastelaro, V. (2009). Synthesis and thermal decomposition of SrTi 1-x Fe x O 3 ($0.0 \leq x \leq 0.1$) powders obtained by the polymeric precursor method. Journal of thermal analysis and calorimetry, 97(1), 173-177. [CrossRef]

[49] Posadas, A. B., Lin, C., Demkov, A. A., & Zollner, S. (2013). Bandgap engineering in perovskite oxides: Al-doped SrTiO3. *Applied Physics Letters, 103*(14). [CrossRef]

[50] Mahesh Kumar, M., & Post, M. L. (2005). Effect of grain boundaries on hydrocarbon sensing in Fe-doped p-type semiconducting perovskite SrTiO3 films. *Journal of applied physics, 97*(11). [CrossRef]

[51] Wang, X., Wang, Z., Hu, Q., Zhang, C., Wang, D., & Li, L. (2019). Room temperature multiferroic properties

of Fe-doped nonstoichiometric SrTiO3 ceramics at both A and B sites. *Solid State Communications, 289*, 22-26. [CrossRef]

[52] Li, J. C., Zhang, C., Zhang, R. Z., Wang, C. L., Zhang, J. L., Zhao, M. L., & Mei, L. M. (2007, June). Electronic structure and thermoelectric properties of Fe-doped BaTiO 3 and SrTiO 3. In *2007 26th International Conference on Thermoelectrics* (pp. 175-179). IEEE. [CrossRef]

[53] Kim, H. S., Bi, L., Dionne, G. F., & Ross, C. A. (2008). Magnetic and magneto-optical properties of Fe-doped SrTiO3 films. *Applied Physics Letters, 93*(9). [CrossRef]

[54] Sikam, P., Thirayatorn, R., Kaewmaraya, T., Thongbai, P., Moontragoon, P., & Ikonic, Z. (2022). Improved thermoelectric properties of SrTiO3 via (La, Dy and N) co-doping: DFT approach. *Molecules, 27*(22), 7923. [CrossRef]

[55] Yu, Z., Ang, C., Vilarinho, P. M., Mantas, P. Q., & Baptista, J. L. (1998). Dielectric properties of Bi doped SrTiO 3 ceramics in the temperature range 500–800 K. *Journal of applied physics, 83*(9), 4874-4877. [CrossRef]

[56] Mehdizadeh Dehkordi, A., Bhattacharya, S., Darroudi, T., Graff, J. W., Schwingenschlogl, U., Alshareef, H. N., & Tritt, T. M. (2014). Large thermoelectric power factor in Pr-doped SrTiO3-δ ceramics via grain-boundary-induced mobility enhancement. *Chemistry of Materials, 26*(7), 2478–2485. [CrossRef]

[57] Sereda, V. V., Tsvetkov, D. S., Sereda, A. V., Malyshkin, D. A., Ivanov, I. L., & Zuev, A. Y. (2025). Enthalpy increments and redox energetics of titanium-substituted strontium ferrites $SrTi_{1-x}Fe_xO_3$-δ. *Journal of Alloys and Compounds, 1010*, 177780. [CrossRef]

[58] Kumar, A. S., Suresh, P., Kumar, M. M., Srikanth, H., Post, M. L., Sahner, K., ... & Srinath, S. (2010, January). Magnetic and ferroelectric properties of Fe doped SrTiO3-δ films. In Journal of Physics: Conference Series (Vol. 200, No. 9, p. 092010). [CrossRef]

[59] Kim, D. H., Aimon, N. M., Bi, L., Dionne, G. F., & Ross, C. A. (2012). The role of deposition conditions on the structure and magnetic properties of $SrTi_{1-x}Fe_xO_3$ films. *Journal of Applied Physics, 111*(7). [CrossRef]

[60] Navarro, A. M. M., Torres, C. E. R., Nomura, K., Takahashi, M., & Errico, L. (2024). The role of the dopants and oxygen vacancies in the magnetic response of Fe-doped and (Fe, Sn) co-doped SrTiO3 perovskite oxide. *Interactions, 245*(1), 21. [CrossRef]

[61] Jose, R., & Vijay, A. (2022). Tuning thermoelectric properties of Nb and Ta co-doped SrTiO3 ceramics. *Materials Today: Proceedings, 64*, 464-467. [CrossRef]

[62] Li, R., Zhang, C., Liu, J., Zhou, J., & Xu, L. (2019). Effect of B-site deficiency on the (In, Fe) co-doped SrTiO3. *Applied Physics A, 125*(11), 773. [CrossRef]

[63] Chotsawat, M., Saiyasombat, C., Busayaporn, W., Sikam, P., Thirayatorn, R., Nachaithong, T., ... & Moontragoon, P. (2026). Effect of nature and formation of defects to optical, magnetic and dielectric properties in Co-doped SrTiO3: DFT and experiments approaches. *Ceramics International*. [CrossRef]

[64] Chao, Z., Chun-Lei, W., Ji-Chao, L., & Kun, Y. (2007). Structural and electronic properties of Fe-doped BaTiO3 and SrTiO3. *Chinese physics, 16*(5), 1422-1428. [CrossRef]

[65] Popuri, S. R., Decourt, R., Mcnulty, J. A., Pollet, M., Fortes, A. D., Morrison, F. D., ... & Bos, J. W. G. (2019). Phonon–glass and heterogeneous electrical transport in A-site-deficient SrTiO3. *The Journal of Physical Chemistry C, 123*(9), 5198-5208. [CrossRef]

[66] Dresselhaus, M. S., Chen, G., Tang, M. Y., Yang, R. G., Lee, H., Wang, D. Z., ... & Gogna, P. (2007). New directions for low-dimensional thermoelectric materials. *Advanced materials, 19*(8), 1043-1053. [CrossRef]

[67] Kovalevsky, A. V., Yaremchenko, A. A., Populoh, S., Weidenkaff, A., & Frade, J. R. (2013). Enhancement of thermoelectric performance in strontium titanate by praseodymium substitution. *Journal of Applied Physics, 113*(5). [CrossRef]

[68] Huang, J., Yan, P., Liu, Y., Xing, J., Gu, H., Fan, Y., & Jiang, W. (2020). Simultaneously breaking the double Schottky barrier and phonon transport in SrTiO3-based thermoelectric ceramics via two-step reduction. *ACS Applied Materials & Interfaces, 12*(47), 52721-52730. [CrossRef]

[69] Riffat, S. B., & Ma, X. (2003). Thermoelectrics: A review of present and potential applications. *Applied Thermal Engineering, 23*(8), 913–935. [CrossRef]

[70] Mroziński, A., Molin, S., & Jasiński, P. (2020). Effect of sintering temperature on electrochemical performance of porous SrTi1-x Fe x O3-δ (x= 0.35, 0.5, 0.7) oxygen electrodes for solid oxide cells. *Journal of Solid State Electrochemistry, 24*(4), 873-882. [CrossRef]

[71] Wang, X., Hu, Q., Zang, G., Zhang, C., & Li, L. (2017). Structural and electrical characteristics of Sr/Ti nonstoichiometric SrTiO3 ceramics. *Solid State Communications, 266*, 1-5. [CrossRef]

[72] Lu, Y., Xu, Z., Wei, L., Chen, H., & Lu, Q. (2025). Establishing Quantitative Understanding of Defect-Tuned Properties in Functional Oxides by an Electrochemically-Induced Gradient of Ionic Defect Concentration. *ACS Applied Materials & Interfaces, 17*(9), 13342-13357. [CrossRef]

[73] Kim, K. T., Kim, C., Fang, S. P., & Yoon, Y. K. (2014). Room temperature multiferroic properties of (Fex, Sr1-x) TiO3 thin films. *Applied Physics Letters, 105*(10). [CrossRef]

[74] Silva, L. F. D. (2009). *Síntese e caracterização do composto $SrTi_{1-x}Fe_xO_3$ nanoestruturado* (Doctoral dissertation, Universidade de São Paulo).

[75] Borup, K. A., De Boor, J., Wang, H., Drymiotis, F., Gascoin, F., Shi, X., ... & Snyder, G. J. (2015). Measuring thermoelectric transport properties of

materials. *Energy & Environmental Science, 8*(2), 423-435. [CrossRef]

[76] Ang, C., Yu, Z., Jing, Z., Lunkenheimer, P., & Loidl, A. (2000). Dielectric spectra and electrical conduction in Fe-doped SrTiO 3. *Physical Review B, 61*(6), 3922. [CrossRef]

[77] Kovalevsky, A. V., Populoh, S., Patrício, S. G., Thiel, P., Ferro, M. C., Fagg, D. P., ... & Weidenkaff, A. (2015). Design of SrTiO3-based thermoelectrics by tungsten substitution. *The Journal of Physical Chemistry C, 119*(9), 4466-4478. [CrossRef]

[78] Ren, G., Lan, J., Zeng, C., Liu, Y., Zhan, B., Butt, S., ... & Nan, C. W. (2015). High performance oxides-based thermoelectric materials. *Jom, 67*(1), 211-221. [CrossRef]

[79] Kovalevsky, A. V., Yaremchenko, A. A., Populoh, S., Thiel, P., Fagg, D. P., Weidenkaff, A., & Frade, J. R. (2014). Towards a high thermoelectric performance in rare-earth substituted SrTiO 3: effects provided by strongly-reducing sintering conditions. *Physical Chemistry Chemical Physics, 16*(48), 26946-26954. [CrossRef]

[80] Fergus, J. W. (2012). Oxide materials for high temperature thermoelectric energy conversion. *Journal of the European Ceramic Society, 32*(3), 525-540. [CrossRef]

[81] Suzuki, I., Gura, L., & Klein, A. (2019). The energy level of the Fe 2+/3+-transition in BaTiO 3 and SrTiO 3 single crystals. *Physical Chemistry Chemical Physics, 21*(11), 6238-6246. [CrossRef]

[82] Varghese, R., Jose, S. M., Thomas, J. K., & Babu, S. C. (2025). Fe-dopinginduced optical, electrical, and dielectric property enhancement in strontium titanate. *Journal of Materials Science: Materials in Electronics, 36*(23), 1428. [CrossRef]

[83] Taibl, S., Fafilek, G., & Fleig, J. (2016). Impedance spectra of Fe-doped SrTiO 3 thin films upon bias voltage: inductive loops as a trace of ion motion. *Nanoscale, 8*(29), 13954-13966. [CrossRef]

[84] Fuentes, S., Muñoz, P., Barraza, N., Chávez-Angel, E., & Sotomayor Torres, C. M. (2015). Structural characterisation of slightly Fe-doped SrTiO3 grown via a sol–gel hydrothermal synthesis. *Journal of Sol-Gel Science and Technology, 75*(3), 593-601. [CrossRef]

[85] Kurt, O., Ascienzo, D., Greenbaum, S., Bayer, T. J. M., Randall, C. A., Madamopoulos, N., & Ren, Y. H. (2017). Nonlinear optical detections of structural distortions at degraded Fe-doped SrTiO3 interfaces. *Materials Chemistry and Physics, 198*, 131-136. [CrossRef]

[86] Dong, X. L., Zhang, K. H., & Xu, M. X. (2018). First-principles study of electronic structure and magnetic properties of SrTi1-x M x O3 (M= Cr, Mn, Fe, Co, or Ni). *Frontiers of Physics, 13*(5), 137106. [CrossRef]

[87] Paul, P. C., Mahato, D. K., & Mahato, M. (2025). Fe-doped SrTiO3 perovskites: exploring their applications in photocatalytic dye degradation and supercapacitors. *Frontiers of Materials Science, 19*(2), 250719. [CrossRef]

[88] Sikam, P., Sararat, C., Moontragoon, P., Kaewmaraya, T., & Maensiri, S. (2018). Enhanced thermoelectric properties of N-doped ZnO and SrTiO3: A first-principles study. *Applied Surface Science, 446*, 47-58. [CrossRef]

[89] Miruszewski, T., Dzierzgowski, K., Winiarz, P., Wachowski, S., Mielewczyk-Gryń, A., & Gazda, M. (2020). Structural properties and water uptake of $SrTi_{1-x}Fe_xO_3$-x/2-δ. *Materials, 13*(4), 965. [CrossRef]

M. Imran Khan Ph.D Scholar at FUUAST, received the M.S. degree in Physics from NED university of Engineering & Technology 75270, Pakistan, in 2019. (Email: imrankhan25430@gmail.com)

Fayaz Hussain Professor & Chairman Department of Materials Engineering, NED University of Engineering and Technology, 75270, Pakistan. Editorial Board Member of "Ceramics" Journal (JCR), "International Journal of Energy Research", Journal of Frontiers in Materials (JCR), Electro-active Materials (Malaysia), Journal of Advanced Dielectrics Editorial Board, Xian Jiao tong University, China and "Crystals" Journal (JCR). (Email: fhussain@neduet.edu.pk)

Hareem Zubairi was a Research Assistant at NED University of Engineering & Technology, Pakistan. Currently a PhD Scholar at the University of Manchester, England, United Kingdom. (Email: hareem.zubairi@manchester.ac.uk)

Syeda Mahnoor Fatima received the M.E. degree in materials engineering from Department of Materials Engineering, NED University of Engineering and Technology, in 2024. (Email: fatimamahnoor923@gmail.com)

Sajida Shaikh Assistant Professor, Department of Materials Engineering, NED University of Engineering and Technology, Karachi 75270, Pakistan. (Email: sajidashiekh@neduet.edu.pk)

Ikhtiar Hussain Bhellar Assistant Professor in Physics GDBC Gulstan-e-Jauhar Karachi College Education Department Government of Sindh Karachi. received the M.S. degree in Physics from NED university of Engineering & Technology75270, Pakistan, in 2019. (Email: ikhtiarhussainbhellar@gmail.com)

S. Naseem Shah Assistant Professor in Physics. Federal Urdu University of Arts Science & Technology, karachi, Pakistan. (Email: syednaseemshah@fuuast.edu.pk)

Fazli Akram Materials Technologist/ Microscopist, Department of materials and Metallurgical Engineering, New Mexico Institute of Mining and Technology, Scorro, NM 87801, United States. (Email: fazliakramss@hotmail.com)

Mukhtiar Hussain (Ph.D. Scholar BIT) received the M.S. Physics from NED University of Engineering & technology, Karachi 75290, Pakistan, in 2019. (Email: mukhtiarhussain652@gmail.com)

Ahmed Ali Bozdar Lecturer in Government college education department. Received the M.S. degree in Physics from NED university of Engineering & Technology75270, Pakistan, in 2019. (Email: sarmadbalochphys@gmail.com)

Muhammad Fahad Riaz Ph.D. in Materials Engineering from NED University of Engineering and Technology, Karachi, Pakistan & Harbin Institute of Technology (HIT), China. Research area includes dielectric materials, energy storage devices and multi-layer ceramic capacitors (MLCCs). (Email: Fahad.riaz@duet.edu.pk)